Ionic Liquids as Precursors for Efficient Mesoporous Iron-Nitrogen-Doped Oxygen Reduction Electrocatalysts**

Zelong Li, Guanglan Li, Luhua Jiang, Jinlei Li, Gongquan Sun,* Chungu Xia,* and Fuwei Li*

Abstract: *A ferrocene-based ionic liquid (Fe-IL) is used as a metal-containing feedstock with a nitrogen-enriched ionic liquid (N-IL) as a compatible nitrogen content modulator to prepare a novel type of non-precious-metal–nitrogen–carbon (M-N-C) catalysts, which feature ordered mesoporous structure consisting of uniform iron oxide nanoparticles embedded into N-enriched carbons. The catalyst Fe^{10}@NOMC exhibits comparable catalytic activity but superior long-term stability to 20 wt % Pt/C for ORR with four-electron transfer pathway under alkaline conditions. Such outstanding catalytic performance is ascribed to the populated Fe (Fe_3O_4) and N (N2) active sites with synergetic chemical coupling as well as the ordered mesoporous structure and high surface area endowed by both the versatile precursors and the synthetic strategy, which also open new avenues for the development of M-N-C catalytic materials.*

In fuel cells, the oxygen reduction reaction (ORR) is invariably involved at the cathode and currently dominated by Pt-based electrocatalysts, which is also thought as the major obstacle for a widespread deployment of these technologies because of the high cost and limited reserves of Pt.[1] As a consequence, the development of Pt-based alloy[2] and cheaper metal-free[3] and non-precious metal catalysts[4] (such as M-N-C, where M is mainly Fe or Co) with high ORR activity and stability has become a major focus of the fuel-cell research.

Despite some breakthroughs having been achieved by selecting suitable metal, nitrogen, and carbon precursors combined with the optimized synthetic strategies,[5] facile preparation of M-N-C catalysts possessing comparable activ-

ity and durability at low cost with the state-of-the-art Pt/C remains a challenge. In general, the M-N-C catalysts were mainly prepared through direct pyrolyzation of the precursors containing Fe or Co salts, nitrogen, and macrocyclic compounds adsorbed on carbon black.[6] However, it was difficult to efficiently construct strong interaction between the M and N species and control porous structure of the materials. Although the catalytically active sites in M-N-C catalyst remain controversial,[7] it has been confirmed that the N-doping of carbon could assist in a stronger coupling between metal oxide and N-doped carbon, and thus lead to higher ORR activity in alkaline solution.[8] Simultaneously, the design of precursor structure at molecular level can effectively tune the interaction among their components and catalytic properties of materials, enabling enhancement both in activity and durability.[9] Therefore, it is convinced that the development of precursors at molecular level containing M, N, and C resources with high thermal stability is crucial.[10] The porosity and surface area of ORR catalyst are critical for mass transport and exposure of active sites.[11] From this point of view, the hard template method using ordered mesoporous silica (SBA-15) as template can be especially feasible and advantageous for preparing an ordered mesoporous M-N-C catalyst with high specific surface area;[12] furthermore, the formation of a metal-embedded nanophase through hard template synthesis can enhance the stability of metal that doped in carbon.[13]

Recently, ionic liquids (ILs) with negligible volatility and high thermal stability have been approved to be a new type of precursor for the preparation of N-doping carbon materials (Supporting Information, Table S1).[14] Nevertheless, metal-based ionic liquids used as versatile precursors to prepare porous metal-doped carbon materials are rarely reported. Herein, we report our discovery on using the "task-specific" Fe-IL ([FcN][NTf$_2$]) as metal-containing precursor and N-IL ([MCNIm][N(CN)$_2$]) as a compatible nitrogen content modulator to synthesize the Fe-N-doped ordered mesoporous carbon catalysts (Fe^X@NOMC in Scheme 1, where X represents the mass percentage of Fe), among which the Fe^{10}@NOMC exhibits outstanding ORR performance under alkaline conditions.

As shown in Scheme 1, Fe^X@NOMC (X = 25, 10, 5) were prepared from Fe-IL or its homogeneous mixture with N-IL by hard template method (see the Supporting Information). Fe^{25}@NOMC was initially synthesized using pure [FcN][NTf$_2$] as the Fe, N, and C feedstock with 1.4 wt % of N doping revealed by elemental analysis. In contrast to the preparation of Fe^{25}@NOMC, Fe^5@NOMC was obtained by treating the carbon@silica composite with 10 wt % HF aqueous solution, affording 1.8 wt % of N incorporation. Fe^{10}@NOMC with N

[*] Dr. Z. L. Li,[+] J. L. Li, Prof. C. G. Xia, Prof. F. W. Li
State Key Laboratory for Oxo Synthesis and Selective Oxidation
Lanzhou Institute of Chemical Physics
Chinese Academy of Sciences, Lanzhou 730000 (China)
E-mail: cgxia@licp.cas.cn
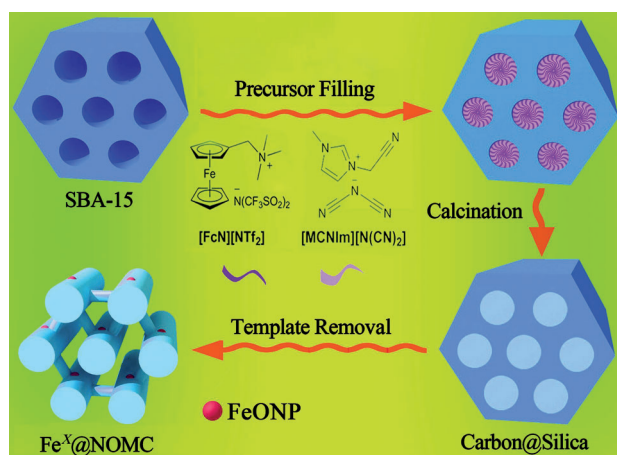   fuweili@licp.cas.cn

Dr. G. L. Li,[+] Prof. L. H. Jiang, Prof. G. Q. Sun
Division of Fuel Cell & Battery
Dalian National Laboratory for Clean Energy
Dalian Institute of Chemical Physics
Chinese Academy of Sciences, Dalian 116023 (China)
E-mail: gqsun@dicp.ac.cn

[+] These authors contributed equally to this work.

1494 **Wiley Online Library**

© 2015 Wiley-VCH Verlag GmbH & Co. KGaA, Weinheim

Angew. Chem. Int. Ed. **2015**, *54*, 1494–1498

Scheme 1. Illustration of the synthesis of Fe^X@NOMC.

Figure 2. TEM (a, d, i), HRTEM (b, e, f), HAADF-STEM (c, g) and elemental mapping (h) images of Fe^{25}@NOMC (a–c), Fe^{10}@NOMC (d–h), and Fe^5@NOMC (i).

contents as high as 11.9 wt% was fabricated by using the mixture of [FcN][NTf$_2$] and [MCNIm][N(CN)$_2$] with 1:1 mass ratio.

The Fe^X@NOMC composites comprise of graphitic carbon, as evidenced by the peak of wide-angle XRD (WAXRD) patterns at around 25°, which corresponds to the diffraction from the (002) index of graphitic carbon (Figure 1 a). Only Fe^{25}@NOMC displays four broad and weak
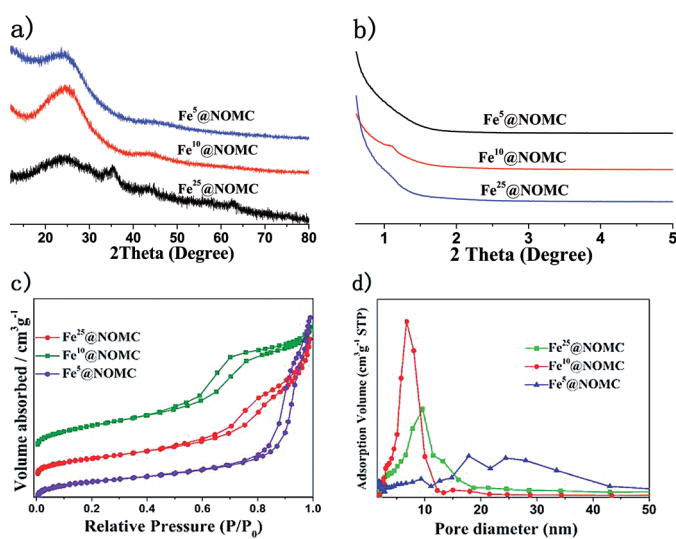

Figure 1. a) WAXRD, b) SAXRD, c) N$_2$ sorption isotherms, and d) the corresponding pore size distribution curves of Fe^{25}@NOMC, Fe^{10}@NOMC, and Fe^5@NOMC.

peaks at around 30.2, 35.6, 43.2, and 62.9°, indicating the formation of γ-Fe$_2$O$_3$ (JCPDS no. 39-1346) nanoparticles (Fe$_2$O$_3$NPs). Although the iron oxide nanoparticles (FeONPs, the coexistence of γ-Fe$_2$O$_3$ and Fe$_3$O$_4$ is verified by the later XPS analysis) in Fe^{25}@NOMC are mostly well-dispersed on the carbon walls revealed by transmission electron microscopy (TEM) and high-angle annular dark-field scanning transmission electron microscopy (HAADF-STEM) (Figure 2 a,c), the aggregated FeONPs are also detected (Figure 2 b). On the
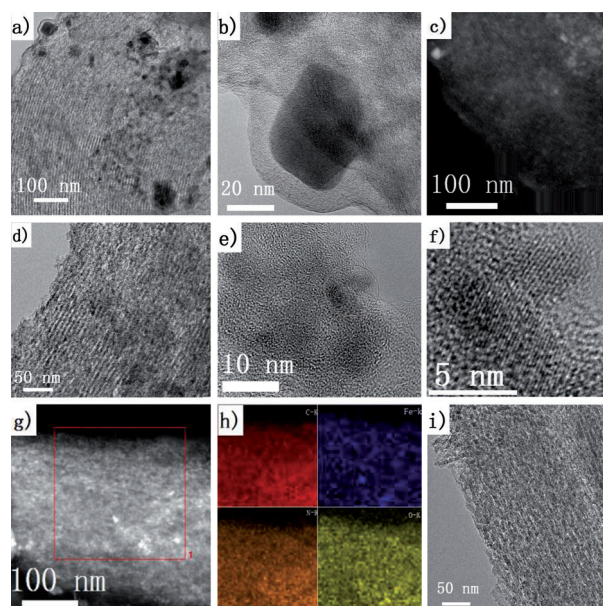
other hand, such FeONPs aggregation is also verified by the appearance of honeycomb pore on the surface of the Fe^5@NOMC after acid leaching (Figure 2 i). The small-angle X-ray diffraction (SAXRD) pattern of the Fe^{25}@NOMC sample shows a weak diffraction peak at about 1° (Figure 1 b), which can be assigned to (100) diffraction of the 2D hexagonal space group (p6mm),[15] suggesting its ordered array of the interconnected Fe-doped NOMC. With the leaching of FeONPs in Fe^5@NOMC, the diffraction peak at 1° disappears, indicating the ordered structure is destroyed.

With the increasing of N content for Fe^{10}@NOMC, the absence of iron phases in the WAXRD patterns together with the evidence of its TEM image might indicate its FeONPs are homogeneously dispersed in the carbonous structure (Figure 2 d), and the intensity of the (100) diffraction peak increases (Figure 1 b). Both XRD and TEM analyses indicate that incorporating more N into carbon can enhance the mesostructure regularity of Fe^{10}@NOMC and promote the FeONP dispersion. Such deduction can also find some clues from their results of N$_2$ sorption isotherms and the pore size distribution. Fe^X@NOMC possess a mesoporous structure (Figure 1 c), high surface areas (411–506 m^2 g^{-1}), and large pore volumes (0.71–1.05 m^3 g^{-1}; Supporting Information, Table S2). The pore size distribution of Fe^{10}@NOMC is highly uniform centered at 5.6 nm (Figure 1 d), which is narrower than that of Fe^{25}@NOMC (centered at 6.8 nm). As expected, Fe^5@NOMC presents a broader pore size distribution because of the partially leaching of different sized FeONPs.

HRTEM images show that the most FeONPs of Fe^{10}@NOMC form the embedded nanophase, which has unique semiexposure morphology, with one part of the NPs being partially exposed to pore channels and the other part

being tightly trapped in the carbons (Figure 2 e,f), and the ultrafine FeONPs with uniform particle size are verified by the homogeneous distribution of white dots along the mesoporous carbon walls (Figure 2 g). Elemental mapping analysis reveals that the C, Fe, N, and O in Fe[10]@NOMC are all uniformly distributed (Figure 2 h). It is interesting to note from HAADF-STEM/EDS line scan of Fe[10]@NOMC that the distribution profile of Fe is highly accordant with that of N (Supporting Information, Figure S3), which strongly suggests certain interaction between Fe and N.

As reported previously, the composition of M, N, and their interaction are the key factors determining the catalytic performance of M-N-C catalysts.[16] The Fe 2p XPS spectra for Fe[X]@NOMC are deconvoluted into a higher binding energy (BE) peak II attributed to γ-Fe_2O_3 and a lower BE peak I assigned to the Fe cations of Fe_3O_4 (Fe_3O_4NPs) that coordinated with nitrogen (Fe-N; Supporting Information, Figure S4 and Table S3),[17] and the Fe-N sites possibly constitute the catalytic centers.[18] Notably, the Fe (Fe_3O_4) content in the surface of Fe[10]@NOMC is much higher than that of Fe[5]@NOMC and Fe[25]@NOMC (Supporting Information, Table S3), and the N content in Fe[10]@NOMC is also significantly higher than the others (Supporting Information, Table S4), suggesting the incorporation of more N is beneficial to the formation of Fe_3O_4 with the help of certain Fe nucleation around N and strong Fe-N interaction, thus provides uniform and highly populated active sites in Fe[10]@NOMC. Moreover, the core-level peaks of Fe 2p for Fe[10]@NOMC shift to higher BEs compared with the other two samples, indicating somehow different iron electronic states. The N 1s spectra are deconvoluted to three peaks locating at 398.3 eV (N1), 399.5 eV (N2), and 400.5 eV (N3) (Supporting Information, Figure S5 and Table S4). N1 and N3 are assigned to pyridinic and pyrrolic nitrogen, and N2 is regarded as the nitrogen associated with Fe_3O_4.[19] Interestingly, the N2 content for Fe[5]@NOMC also decreases with the reduction of iron loading by HF etching, experimentally confirming N2 being bonded to Fe.

The electrocatalytic activities of Fe[X]@NOMC toward the ORR were first investigated by linear sweep voltammetry (LSV) using a rotating disk electrode in 0.1M NaOH solution saturated with O_2. For comparison, commercial 20 wt % Pt/C catalyst was also examined under the same conditions.[20] As shown in Figure 3a, both the ORR onset potential and the half-wave potential (0 V vs. MMO) for the Fe[10]@NOMC are closer to that for the Pt/C and comparable to the Fe/Fe_3C-melamine/N-KB composite catalyst (Ar-800) under similar test conditions,[5c] but significantly more positive than that for Fe[5]@NOMC and Fe[25]@NOMC. The facile ORR process over the Fe[10]@NOMC could be due to the increased content of Fe-N2 with the enhancement of N content.

To further clarify the active sites of such Fe-N-C catalysts, a controllable material Fe@FDU[3]-N (FDU[3]-N denotes the N-doped ordered mesoporous carbon) with dispersive γ-Fe_2O_3 and Fe_3O_4 NPs[17a,b] (Supporting Information, Figures S6, S7 a, S8) and high surface area (522 m[2] g^{−1}; Supporting Information, Table S2) was prepared by loading [FcN][NTf2] into the pore of FDU[3]-N and then direct carbonization under N_2 (see the Supporting Information). Unfortunately, Fe@FDU[3]-N is
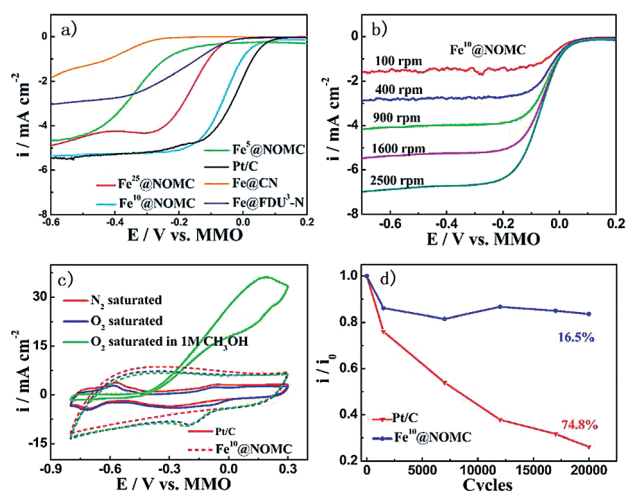

Figure 3. a) RDE voltammetric response for the ORR in O_2-saturated 0.1 M NaOH at a scan rate of 10 mVs[−1]. b) RDE voltammograms recorded for Fe[10]@NOMC electrode in an O_2-saturated 0.1 M NaOH solution with different rotation rates at a scan rate of 10 mVs[−1]. c) CV curves of Fe[10]@NOMC and Pt/C catalysts at a scan rate of 50 mVs[−1] in O_2-or N_2-saturated 0.1 M NaOH solutions as well as O_2-saturated 0.1 M NaOH solution with 1 M CH_3OH. d) Current density degradation at 0 V (vs. Hg/HgO) in the potential cycling process from −0.25 to 0.10 V at a scan rate of 100 mVs[−1].

much less active toward the ORR (Figure 3a). Further XPS analysis of Fe@FDU[3]-N reveals that its nitrogen are mainly in graphitic state (Supporting Information, Figure S9a and Table S4),[21] no N2 species and the crucial Fe-N2 interaction as existence in Fe[X]@NOMC are observed. This result certifies that the post-loading of [FcN][NTf2] into the N-enriched FDU[3]-N cannot generate Fe-N2 interaction, and the formation of Fe-N2 active sites is not only related to the N content but also dependent on the synthetic procedure. Furthermore, Fe@CN with finely dispersive Fe_2C_5 and Fe_3O_4 NPs (Supporting Information, Figures S6, S7b, S10)[22] and high surface area (280 m[2] g^{−1}; Supporting Information, Table S2) was also prepared by direct pyrolysis of [FcN][NTf2] under N_2 (see Supporting Information); however, it displayed more negative onset potential and half-wave potential (Figure 3a) compared with the less-active Fe[25]@NOMC, which is probably due to the negligible interaction between Fe and N (Fe-N2) as observed (Supporting Information, Figure S9b, Table S4). In comparison with the Fe[25]@NOMC, its analogues Fe[5]@NOMC also demonstrated lower ORR reactivity owing to the etching of the Fe species, which leads to the decrease of Fe-N2 active sites. Based on these results, it is concluded that the present synthetic strategy involving the unique Fe-N-C IL precursors and the one-pot synthesis through hard-template can not only generate high surface area and mesoporous structure, but also facilitate the formation of Fe-N2 species, which are all crucial for an efficient ORR catalyst.

To gain more information on the Fe[X]@NOMC-catalyzed ORR, the RDE experiments at different rotating speeds (100–2500 rpm) were performed, and their exact kinetic parameters including the electron-transfer number (n) and the kinetic limiting current (J_k) were calculated on the basis of Koutecky–Levich equation and RDE measurements (Fig-

ure 3b; Supporting Information, Figure S12). Remarkably, the ORR over the Fe[10]@NOMC proceeds via a four-electron transfer pathway ($n = 4$), which is same with that over the Pt/C. While for the Fe[25]@NOMC ($n = 3.7$) and Fe[5]@NOMC ($n = 3.9$), the electron transfer number is a little lower. The J_k value at -0.5 V vs. MMO for Fe[10]@NOMC ($J_k = 5.30$ mA cm^{-2}) is close to that for the Pt/C catalyst ($J_k = 5.38$ mA cm^{-2}) and higher than the values for Fe[25]@NOMC ($J_k = 4.50$ mA cm^{-2}) and Fe[5]@NOMC ($J_k = 4.27$ mA cm^{-2}). In contrast, the electron-transfer number of the Fe@FDU[3]-N and Fe@CN are 2.5 and 2.3, respectively, suggesting a two electron-transfer involving peroxide as the intermediate is dominant in these two ORRs.

Methanol tolerance is a crucial factor for a good ORR catalyst in direct methanol fuel cells. As illustrated in Figure 3c, the Fe[10]@NOMC catalyst showed perfect ORR selectivity in methanol containing electrolyte, whereas a significantly high methanol oxidation current is detected for the Pt/C catalyst under the same conditions. Furthermore, the stabilities of the Fe[10]@NOMC and Pt/C were further evaluated by an accelerated aging test procedure as described in the Supporting Information.[23] After 20000 cycles scanning from -0.25 to 0.10 V, the current density at 0 V vs. MMO only decreased by 16.5% for Fe[10]@NOMC, which is much lower than that of the Pt/C (74.8%) (Figure 3d). Such outstanding stability of the as-prepared Fe[10]@NOMC catalyst might be ascribed to not only the strong interaction between FeONPs and N2 species but also the formation of FeONPs-embedded nanophase that could retard their leaching into the alkaline media during long-term operation.

In summary, a new family of mesoporous Fe-N-C catalyst has been fabricated from versatile and structurally defined Fe-IL/N-IL precursors, the introduction of another IL with high N content as co-precursor can facilely tune the N content of the Fe-N-C catalysts. It was found that doping more N was beneficial to the formation of active Fe (Fe$_3$O$_4$) and N (N2) species as well as enhancement of their interaction. Compared with the post-loading and direct pyrolysis procedures, the synthetic strategy using unique ionic liquid precursors and the one-pot synthesis through hard-template showed significant advantages in the construction of mesoporous morphology with high surface area and the formation of Fe-N2 species, which played important roles in the development of an efficient ORR catalyst. With these crucial characters, Fe[10]@NOMC displayed comparable reaction current density and onset potential with the commercial Pt/C, but much better fuel crossover resistance and long-term durability in alkaline condition. The facile N, M tuning of the present method and outstanding ORR performance of the resultant Fe[10]@NOMC indicate its wide application in the development of M-N-C materials for heterogeneous catalysis, batteries, and supercapacitors.

[1] a) J. Suntivich, H. A. Gasteiger, N. Yabuuchi, H. Nakanishi, J. B. Goodenough, Y. Shao-Horn, *Nat. Chem.* **2011**, *3*, 546–550; b) S. Guo, S. Zhang, S. Sun, *Angew. Chem. Int. Ed.* **2013**, *52*, 8526–8544; *Angew. Chem.* **2013**, *125*, 8686–8705; c) G. Wu, P. Zelenay, *Acc. Chem. Res.* **2013**, *46*, 1878–1889.

[2] a) V. R. Stamenkovic, B. Fowler, B. S. Mun, G. Wang, P. N. Ross, C. A. Lucas, N. M. Marković, *Science* **2007**, *315*, 493–497; b) X. Huang, E. Zhu, Y. Chen, Y. Li, C.-Y. Chiu, Y. Xu, Z. Lin, X. Duan, Y. Huang, *Adv. Mater.* **2013**, *25*, 2974–2979; c) C. Zhang, S. Y. Hwang, A. Trout, Z. Peng, *J. Am. Chem. Soc.* **2014**, *136*, 7805–7808.

[3] a) K. Elumeeva, N. Fechler, T. P. Fellinger, M. Antonietti, *Mater. Horiz.* **2014**, *1*, 588–594; b) D.-W. Wang, D. Su, *Energy Environ. Sci.* **2014**, *7*, 576–591; c) S. G. Zhang, M. S. Miran, A. Ikoma, K. Dokko, M. Watanabe, *J. Am. Chem. Soc.* **2014**, *136*, 1690–1693.

[4] a) J. Tian, A. Morozan, M. T. Sougrati, M. Lefèvre, R. Chenitz, J.-P. Dodelet, D. Jones, F. Jaouen, *Angew. Chem. Int. Ed.* **2013**, *52*, 6867–6870; *Angew. Chem.* **2013**, *125*, 7005–7008; b) D. Zhao, J.-L. Shui, L. R. Grabstanowicz, C. Chen, S. M. Commet, T. Xu, J. Lu, D.-J. Liu, *Adv. Mater.* **2014**, *26*, 1093–1097; c) Y. Zhu, B. Zhang, X. Liu, D.-W. Wang, D. S. Su, *Angew. Chem. Int. Ed.* **2014**, DOI: 10.1002/anie.201405314; *Angew. Chem.* DOI: 10.1002/ange.201405314.

[5] a) M. Lefèvre, E. Proietti, F. Jaouen, J.-P. Dodelet, *Science* **2009**, *324*, 71–74; b) G. Wu, K. L. More, C. M. Johnston, P. Zelenay, *Science* **2011**, *332*, 443–447; c) J.-S. Lee, G. S. Park, S. T. Kim, M. Liu, J. Cho, *Angew. Chem. Int. Ed.* **2013**, *52*, 1026–1030; *Angew. Chem.* **2013**, *125*, 1060–1064; d) J. Masa, W. Xia, I. Sinev, A. Zhao, Z. Sun, S. Grutzke, P. Weide, M. Muhler, W. Schuhmann, *Angew. Chem. Int. Ed.* **2014**, *53*, 8508–8512; *Angew. Chem.* **2014**, *126*, 8648–8652.

[6] a) S. Gupta, D. Tryk, I. Bae, W. Aldred, E. Yeager, *J. Appl. Electrochem.* **1989**, *19*, 19–27; b) H. Schulenburg, S. Stankov, V. Schünemann, J. Radnik, I. Dorbandt, S. Fiechter, P. Bogdanoff, H. Tributsch, *J. Phys. Chem. B* **2003**, *107*, 9034–9041; c) W. Li, A. Yu, D. C. Higgins, B. G. Llanos, Z. Chen, *J. Am. Chem. Soc.* **2010**, *132*, 17056–17058; d) K. Parvez, S. Yang, Y. Hernandez, A. Winter, A. Turchanin, X. Feng, K. Müllen, *ACS Nano* **2012**, *6*, 9541–9550.

[7] a) Y. Liang, Y. Li, H. Wang, H. Dai, *J. Am. Chem. Soc.* **2013**, *135*, 2013–2036; b) Q. Wang, Z.-Y. Zhou, Y.-J. Lai, Y. You, J.-G. Liu, X.-L. Wu, E. Terefe, C. Chen, L. Song, M. Rauf, N. Tian, S.-G. Sun, *J. Am. Chem. Soc.* **2014**, *136*, 10882–10885.

[8] a) Y. Liang, Y. Li, H. Wang, J. Zhou, J. Wang, T. Regier, H. Dai, *Nat. Mater.* **2011**, *10*, 780–786; b) Y. Liang, H. Wang, P. Diao, W. Chang, G. Hong, Y. Li, M. Gong, L. Xie, J. Zhou, J. Wang, T. Z. Regier, F. Wei, H. Dai, *J. Am. Chem. Soc.* **2012**, *134*, 15849–15857.

[9] a) R. Murugavel, M. G. Walawalkar, M. Dan, H. W. Roesky, C. N. R. Rao, *Acc. Chem. Res.* **2004**, *37*, 763–774; b) C. Chen, Y. Kang, Z. Huo, Z. Zhu, W. Huang, H. L. Xin, J. D. Snyder, D. Li, J. A. Herron, M. Mavrikakis, M. Chi, K. L. More, Y. Li, N. M. Markovic, G. A. Somorjai, P. Yang, V. R. Stamenkovic, *Science* **2014**, *343*, 1339–1343.

[10] a) Z. Li, J. Liu, Z. Huang, Y. Yang, C. Xia, F. Li, *ACS Catal.* **2013**, *3*, 839–845; b) P. Su, H. Xiao, J. Zhao, Y. Yao, Z. Shao, C. Li, Q. Yang, *Chem. Sci.* **2013**, *4*, 2941–2946.

[11] a) Z.-S. Wu, S. Yang, Y. Sun, K. Parvez, X. Feng, K. Müllen, *J. Am. Chem. Soc.* **2012**, *134*, 9082–9085; b) A. Kong, X. Zhu, Z. Han, Y. Yu, Y. Zhang, B. Dong, Y. Shan, *ACS Catal.* **2014**, *4*, 1793–1800.

[12] H.-W. Liang, W. Wei, Z.-S. Wu, X. Feng, K. Müllen, *J. Am. Chem. Soc.* **2013**, *135*, 16002–16005.

[13] Z. Wu, Y. Lv, Y. Xia, P. A. Webley, D. Zhao, *J. Am. Chem. Soc.* **2012**, *134*, 2236–2245.

[14] a) J. S. Lee, X. Wang, H. Luo, G. A. Baker, S. Dai, *J. Am. Chem. Soc.* **2009**, *131*, 4596–4597; b) W. Yang, T.-P. Fellinger, M. Antonietti, *J. Am. Chem. Soc.* **2011**, *133*, 206–209; c) D.-C. Guo, J. Mi, G.-P. Hao, W. Dong, G. Xiong, W.-C. Li, A.-H. Lu, *Energy Environ. Sci.* **2013**, *6*, 652–659.

[15] S. Jun, S. H. Joo, R. Ryoo, M. Kruk, M. Jaroniec, Z. Liu, T. Ohsuna, O. Terasaki, *J. Am. Chem. Soc.* **2000**, *122*, 10712–10713.

[16] a) X. Fu, Y. Liu, X. Cao, J. Jin, Q. Liu, J. Zhang, *Appl. Catal. B* **2013**, *130–131*, 143–151; b) A. Zhao, J. Masa, W. Xia, A. Maljusch, M.-G. Willinger, G. Clavel, K. Xie, R. Schlögl, W. Schuhmann, M. Muhler, *J. Am. Chem. Soc.* **2014**, *136*, 7551–7554.

[17] a) D. Zhang, Z. Liu, S. Han, C. Li, B. Lei, M. P. Stewart, J. M. Tour, C. Zhou, *Nano Lett.* **2004**, *4*, 2151–2155; b) J. Lu, X. Jiao, D. Chen, W. Li, *J. Phys. Chem. C* **2009**, *113*, 4012–4017; c) Z. Wu, W. Li, P. A. Webley, D. Zhao, *Adv. Mater.* **2012**, *24*, 485–491.

[18] a) Y. Zhao, K. Watanabe, K. Hashimoto, *J. Am. Chem. Soc.* **2012**, *134*, 19528–19531; b) Y. Zhao, K. Watanabe, K. Hashimoto, *J. Mater. Chem. A* **2013**, *1*, 1450–1456.

[19] a) M. Ferrandon, A. J. Kropf, D. J. Myers, K. Artyushkova, U. Kramm, P. Bogdanoff, G. Wu, C. M. Johnston, P. Zelenay, *J. Phys. Chem. C* **2012**, *116*, 16001–16013; b) W. Li, J. Wu, D. C. Higgins, J.-Y. Choi, Z. Chen, *ACS Catal.* **2012**, *2*, 2761–2768.

[20] Y. Li, Y. Li, E. Zhu, T. McLouth, C.-Y. Chiu, X. Huang, Y. Huang, *J. Am. Chem. Soc.* **2012**, *134*, 12326–12329.

[21] H. Wang, T. Maiyalagan, X. Wang, *ACS Catal.* **2012**, *2*, 781–794.

[22] C. Yang, H. Zhao, Y. Hou, D. Ma, *J. Am. Chem. Soc.* **2012**, *134*, 15814–15821.

[23] a) Y. J. Sa, C. Park, H. Y. Jeong, S.-H. Park, Z. Lee, K. T. Kim, G.-G. Park, S. H. Joo, *Angew. Chem.* **2014**, *126*, 4186–4190; *Angew. Chem. Int. Ed.* **2014**, *53*, 4102–4106; b) W. Wei, H. Liang, K. Parvez, X. Zhuang, X. Feng, K. Müllen, *Angew. Chem.* **2014**, *126*, 1596–1600; *Angew. Chem. Int. Ed.* **2014**, *53*, 1570–1574.